### nature water

**Analysis** 

https://doi.org/10.1038/s44221-023-00037-0

## Performance metrics for nanofiltrationbased selective separation for resource extraction and recovery

Received: 17 August 2022

Accepted: 27 January 2023

Published online: 9 March 2023



Ruoyu Wang  $m{0}^1$ , Rongrong He $^2$ , Tao He $^2$ , Menachem Elimelech  $m{0}^3$  & Shihong Lin  $m{0}^{1,4} \boxtimes$ 

Membrane filtration has been widely adopted in various water treatment applications, but its use in selective solute separation for resource extraction and recovery is an emerging research area. When a membrane process is applied for solute-solute separation to extract solutes as the product, the performance metrics and process optimization strategies should differ from a membrane process for water production because the separation goals are fundamentally different. Here we used lithium (Li) magnesium (Mg) separation as a representative solute-solute separation to illustrate the deficiency of existing performance evaluation framework developed for water-solute separation using nanofiltration (NF). We performed coupon- and module-scale analyses of mass transfer to elucidate how membrane properties and operating conditions affect the performance of Li/Mg separation in NF. Notably, we identified an important operational trade-off between Li/Mg selectivity and Li recovery, which is critical for process optimization. We also established a new framework for evaluating membrane performance based on the success criteria of Li purity and recovery and further extended this framework to separation with the target ions in the brine. This analysis lays the theoretical foundation for performance evaluation and process optimization for NF-based selective solute separation.

Selective solute–solute separation has become a research frontier due to its potential applications in resource extraction and recovery<sup>1,2</sup>. The technological progress in membrane-based solute–water separation over the past half century, particularly in reverse osmosis (RO) and nanofiltration (NF), has enabled energy-efficient desalination and water purification<sup>3,4</sup>. In those applications, water is the primary product whereas the solutes are the unwanted constituents rejected by membranes (Fig. 1a). In seawater or brackish water desalination, the rejected solutes are mainly salts, while in wastewater re-use, the rejected solutes include both salts and organic substances. The ideal

membranes for these applications should have a high water–solute selectivity, that is, they should have high water permeability while maintaining low solute permeability, leading to fast water production and high solute rejection<sup>3,5</sup>. Extensive efforts have been devoted to developing membranes with high water–solute selectivity<sup>5,6</sup>. So far, commercial RO/NF membranes have adequate water–solute selectivities for delivering reasonably good performance in desalination and water purification<sup>7,8</sup>.

As RO membranes reject most solutes to a great extent and indiscriminately, pressure-driven membrane-based selective solute–solute

<sup>1</sup>Department of Civil and Environmental Engineering, Vanderbilt University, Nashville, TN, USA. <sup>2</sup>Shanghai Advanced Research Institute, Chinese Academy of Sciences, Shanghai, China. <sup>3</sup>Department of Chemical and Environmental Engineering, Yale University, New Haven, CT, USA. <sup>4</sup>Department of Chemical and Biomolecular Engineering, Vanderbilt University, Nashville, TN, USA. ⊠e-mail: shihong.lin@vanderbilt.edu

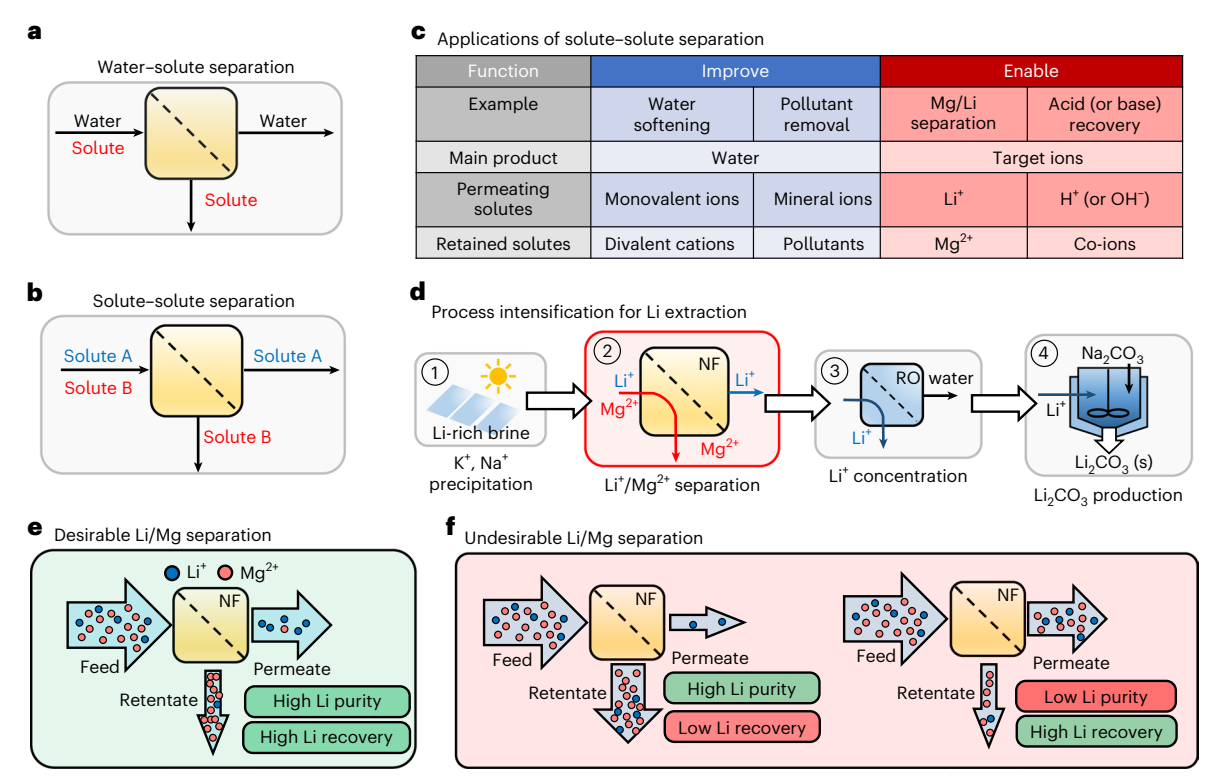


**Fig. 1**| **NF-based solute-solute separation and success criteria. a**, Illustration of conventional water-solute separation. Water is the primary product, whereas the solutes are the unwanted constituents to be rejected by membranes. **b**, Illustration of solute-solute separation. Certain target solutes are allowed to pass through, while the others are retained by membranes. **c**, Representative applications of selective solute-solute separation classified into two categories: improvement and enablement. Examples of the improvement category include NF-based water softening and micropollutant removal, where the primary product is water. Examples of the enablement category include acid (or base) recovery and Li/Mg separation, where the primary product is target solute.

separation relies on NF that differentiates the rejections of solutes on the basis of their physicochemical properties (Fig. 1b). In general, NF-based solute–solute separation can be classified into two major categories (Fig. 1c). In the first category, the primary product is water, and the role of solute–solute separation is to improve the NF-based water treatment processes. For instance, in NF-based water softening, hardness ions (Ca²+ and Mg²+) are rejected whereas monovalent ions (for example, Na+ and K+) can readily pass through  $^{9,10}$ . NF has also been used to selectively remove micropollutants without removing benign mineral ions  $^{11,12}$ . The ability to achieve selective solute–solute separation in these contexts can lead to a desired product water quality (for example, reserving nutrient ions for fertigation), prevention of mineral scaling in subsequent desalination processes, and/or energy saving via reducing transmembrane osmotic pressure difference.

The second category of NF-based selective solute–solute separation aims at enabling the extraction of target solutes as the primary product. For example, when strong acid or base is used to recover cationic or anionic adsorbates from polymeric or mineral adsorbents, NF can be applied to concentrate the adsorbates (in the retentate) and recover acid or base (in the permeate) for re-use. A similar application of this type is dye recovery from textile wastewater, where dye molecules are retained and concentrated as the target solutes<sup>13</sup>. One potentially prominent NF application of the second category is lithium (Li) extraction from brines rich in magnesium (Mg)<sup>14</sup>.

The conventional method for Li production from brine is based on evaporation and chemical precipitation, which typically requires that

the brine has a low Mg-to-Li ratio (MLR) <sup>15,16</sup>. In recent years, integration of membrane processes into the treatment trains has received increasing interest for process intensification, and for enabling Li extraction from brines with a high MLR <sup>14</sup>. A representative treatment train includes an evaporative process for precipitating out Na and K salts, an NF process for separating Li and Mg, an RO process to concentrate the Li-rich NF permeate, and a final precipitation process for generating Li  $_2\mathrm{CO}_3$  as the product (Fig. 1d) <sup>17</sup>. NF-based Li/Mg separation is the most critical and technically challenging unit process in such a treatment train. Thus, many efforts have been devoted in recent years to developing high-performance NF membranes for Li/Mg separation <sup>18-24</sup>.

But what exactly is a good NF membrane for Li/Mg separation, or more generally, for any solute–solute separation? As the treatment goal is no longer simple separation of solute from water, the conventional framework of membrane evaluation based on water–solute selectivity is insufficient. In most papers on developing solute–solute separation membranes, performance was evaluated on the basis of solute–solute selectivity and water permeability  $^{18-24}$ . The selectivity of solute A over solute B,  $S_{\rm A/B}$ , is defined as  $^{25}$ 

$$S_{A/B} \equiv \frac{1 - R_A}{1 - R_B} = \frac{J_A/c_{f,A}}{J_B/c_{f,B}}$$
 (1)

where  $R_A$  ( $R_B$ ),  $J_A$  ( $J_B$ ) and  $c_{f,A}$  ( $c_{f,B}$ ) are the apparent rejection, solute flux and feed concentration of solute A (or B), respectively.  $S_{A/B}$  is also called separation factor. The solute flux and feed concentration can be based

on either mass or mole as long as the concentrations are consistent within the equation. In the following discussion, we will use mass-based definitions as adopted by most literature, although mole-based definitions are mechanistically more meaningful.

In this Analysis, we will show that  $S_{A/B}$  alone is insufficient for evaluating an NF membrane or process for selective solute–solute separations for resource recovery. While the principle should be generally applicable, we focus the current analysis on the specific application of Li/Mg separation to provide a concrete illustration. We start our analysis by evaluating the success criteria for Li/Mg separation and provide a critical analysis of literature data. We then perform coupon- and module-scale analysis to elucidate important operating and material considerations in NF-based Li/Mg separation. Finally, we introduce and discuss two important trade-offs that will guide future process optimization and membrane development to achieve high-performance Li/Mg separation.

#### Why is selectivity not a sufficient metric?

Assessing the adequacy of the metric  $S_{A/B}$  requires first defining a successful Li/Mg separation. As the purpose of the separation is to extract Li from a Li/Mg mixture, the success criteria should have two aspects: purity and recovery (Fig. 1e). Considering a simplified scenario with only Li<sup>+</sup> and Mg<sup>2+</sup> cations, the permeate Li purity,  $\eta_{\text{Li}}$ , is defined as the mass fraction of cations in the permeate that are Li<sup>+</sup>:

$$\eta_{\rm Li} \equiv \frac{c_{\rm p,Li}}{c_{\rm p,Li} + c_{\rm p,Mg}} \tag{2}$$

where  $c_{\rm p,Li}$  and  $c_{\rm p,Mg}$  are the Li<sup>+</sup> and Mg<sup>2+</sup> concentrations in the permeate, respectively. The importance of Li purity is obvious as improving Li purity is the motivation for performing Li/Mg separation. A permeate with low Li purity will result in Li<sub>2</sub>CO<sub>3</sub> precipitate containing an unacceptable level of MgCO<sub>3</sub> impurity. For a feed solution of a given MLR,  $\eta_{\rm Li}$  relates to the Li/Mg selectivity,  $S_{\rm Li/Mg}$ , via the following equation:

$$\eta_{\rm Li} = \frac{1}{1 + {\rm MLR}/S_{\rm Li/Mg}} \tag{3}$$

The second important success criterion is Li recovery, defined as the mass fraction of Li $^{\dagger}$  in the feed that is eventually recovered in the permeate. Specifically, Li recovery, LiR, can be quantified as

$$LiR \equiv \frac{Q_p c_{p,Li}}{Q_f c_{f,Li}} = WR(1 - R_{Li})$$
 (4)

where  $Q_p$  and  $Q_f$  are the volumetric permeate flowrate and influent flowrate of the feed stream, respectively;  $c_{p,Li}$  and  $c_{f,Li}$  are the Li concentrations in the permeate and feed influent, respectively; WR is water recovery; and  $R_{Li}$  is Li rejection. Both WR and  $R_{Li}$  are module-scale performance metrics. As we will show shortly, using  $R_{Li}$  evaluated with membrane coupons for module-scale analysis can lead to inaccurate or even unphysical results. With the definitions of Li purity and recovery, it becomes apparent that a successful Li/Mg separation should recover the majority of Li from the feed solution and at the same time produce a permeate with a high Li purity (Fig. 1e). In other words, attaining only high Li recovery or high Li purity alone is undesirable for the purpose of Li extraction (Fig. 1f).

We summarize and analyse literature data on the performance of NF membranes for Li/Mg separation. We also tested the performance of several commercial membranes (NFX, NF90 and NF270; Supplementary Table 1) to benchmark performance comparison. Both the literature data and results from our experiments are compiled in Fig. 2a–d (see also Supplementary Table 2). The feed MLR spans a wide range from 5:1 to 120:1, and the Mg<sup>2+</sup> concentrations vary by nearly two orders of magnitude (Fig. 2a). The feed

composition is critical as it affects Li/Mg selectivity and directly impacts Li purity via equation (3).

The rejections of Li<sup>+</sup> and Mg<sup>2+</sup> span a wide range of values (Fig. 2b). The rejections of Mg<sup>2+</sup> are typically higher than 70% and can even reach 99.9%. The Li<sup>+</sup> rejection ( $R_{\rm Li}$ ) varies from –140% to 87%. Negative rejection of highly permeable ions (Li<sup>+</sup>) is a result of maintaining Donnan equilibrium and is common in NF when the feed solution mixture has an abundance of strongly rejected co-ions (Mg<sup>2+</sup>) and counter-ions that can easily permeate through the membrane (Cl<sup>-</sup>) (refs. <sup>10,26,27</sup>). The permeation of Cl<sup>-</sup> promotes the transport of the highly permeable cation, Li<sup>+</sup>, to maintain charge neutrality in the permeate solution, thereby resulting in a permeate with even higher Li<sup>+</sup> concentration than that of the feed.

The Li/Mg selectivity,  $S_{\text{Li/Mg}}$ , is strongly sensitive to  $\text{Mg}^{2^+}$  rejection, especially when  $\text{Mg}^{2^+}$  rejection is high (Fig. 2c). This dependence is also obvious from the definition of  $S_{\text{Li/Mg}}$  (equation (1)) in which the denominator is  $1-R_{\text{Mg}}$ . The Li/Mg selectivity and the feed MLR together determine the permeate Li purity, which ranges from below 10% to over 90% (Fig. 2d). The high sensitivity of  $S_{\text{Li/Mg}}$  to  $R_{\text{Mg}}$  suggests that a very high  $S_{\text{Li/Mg}}$  can be achieved even if Li<sup>+</sup> ions are well rejected, provided that  $\text{Mg}^{2^+}$  rejection is near perfect. This property of  $S_{\text{Li/Mg}}$  renders it an insufficient performance metric as it overlooks the factor of Li recovery.

To illustrate the inadequacy of selectivity as a performance metric, a heuristic comparison between two scenarios with the exact same Li/Mg selectivity (50) is provided in Table 1. Two different separations with the same selectivity fall on the same Li/Mg selectivity line in Fig. 2b. The  $R_{\rm Li}$  and  $R_{\rm Mg}$  are -80% and 96.4%, respectively, in the first scenario, and 95% and 99.9% in the second scenario. Li recovery, LiR, is estimated by equation (4) to be 90% for the first scenario but only 2.5% for second scenario when WR is 50%. The extreme difference of LiR for the two separations with the same Li/Mg selectivity clearly demonstrates why selectivity is an inadequate metric. Because of the high sensitivity of Li/Mg selectivity to  $R_{\rm Mg}$ , especially when  $R_{\rm Mg}$  approaches 100%, a very high Li/Mg selectivity can be achieved even when  $R_{\rm Li}$  is unacceptably high for any Li recovery.

Notably, applying equation (4) with a WR of 80% in the first scenario predicts an unphysical LiR of 144%. The emergence of this unphysical prediction is attributable to the implicit use of  $R_{\rm Li}$  measured using coupon-scale experiments in an equation (equation (4)) that should use  $R_{\rm Li}$  of module-scale processes. While an  $R_{\rm Li}$  of -80% is not uncommon in literature (Fig. 2b), those reported  $R_{\rm Li}$  values were measured using membrane coupons (that is, WR is nearly zero) with a certain feed solution composition. To achieve a WR of 80% with membrane modules, however, the feed composition varies along the module due to the selective transport of water and ions. As we will show,  $R_{\rm Li}$  of a module-scale process cannot be highly negative. In other words, an LiR > 100% should not emerge in a module-scale analysis that correctly captures the mass transfer behaviour, which is the focus of the next section.

## Module-scale analysis of NF-based Li/Mg separation

Performing module-scale analysis requires a model to describe the local mass transfer in a differential element of the module. Such a model outputs the local fluxes of water and ions using applied pressure and local feed composition as the inputs. The module behaviour can then be modelled via finite difference method to relate mass transfer in differential elements (for details, see Methods). In this analysis, we employ the solution-diffusion–electromigration (SDEM) model due to its simplicity and ability to model fluxes of multiple components. The SDEM model assumes that any point inside the membrane is in thermodynamic equilibrium with a virtual bulk electrolyte solution that is charge neutral <sup>27–29</sup>. The virtual solution treatment is equivalent to applying a modified Nernst–Planck equation with the ion diffusion coefficient replaced by the ion permeability, which is the product of the

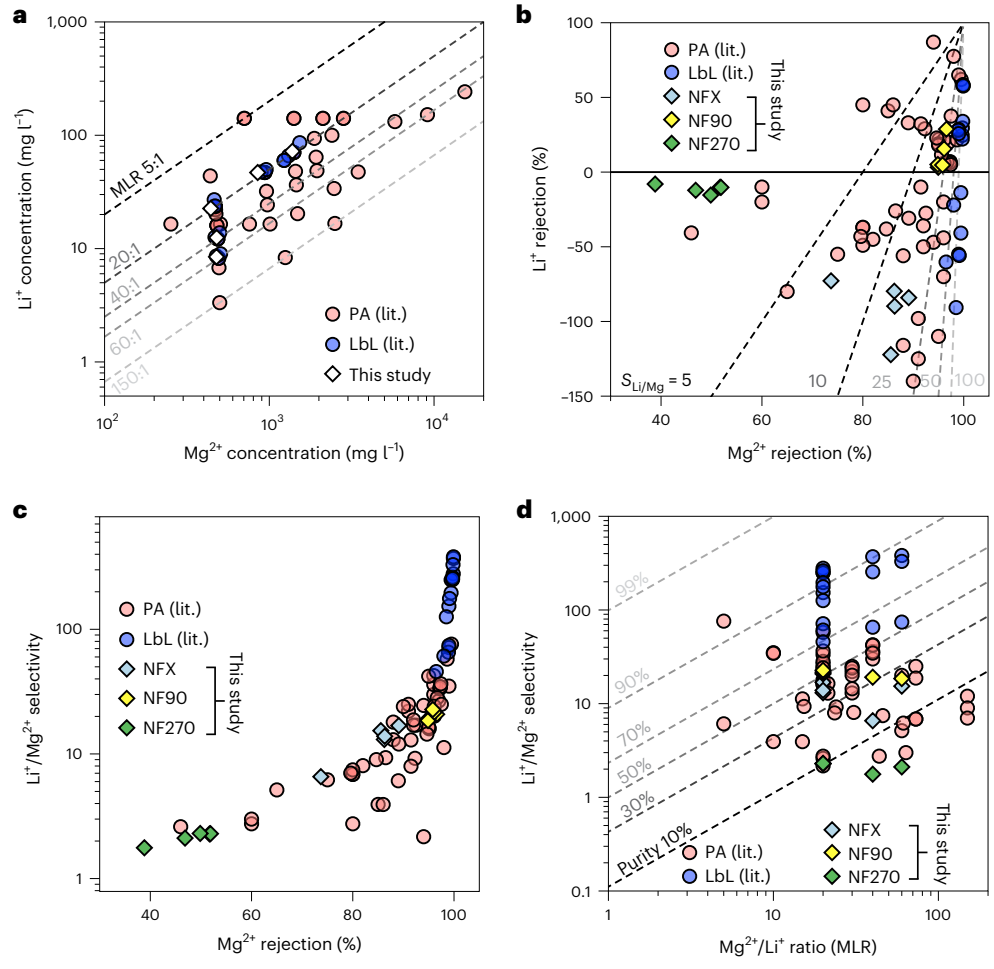


**Fig. 2** | **Summary of membrane performance for NF-based Li/Mg separation. a**, Li<sup>+</sup> and Mg<sup>2+</sup> concentrations of the feed waters used in this study and studies reported in the literature, with the Mg<sup>2+</sup>/Li<sup>+</sup> mass ratios (MLR) presented in dashed lines (vary from 5:1 to 150:1). Data points on the same dash line have the same MLR. **b**, Li<sup>+</sup> and Mg<sup>2+</sup> rejections of three commercial NF membranes tested in this study (NFX, NF90 and NF270) and membranes reported in the literature, with Li<sup>+</sup>/Mg<sup>2+</sup> selectivity (defined by equation (1)) values presented in dashed lines (vary from 5 to 100). Data points on the same dash line have the same Li<sup>+</sup>/Mg<sup>2+</sup> selectivity. **c**, Li<sup>+</sup>/Mg<sup>2+</sup> selectivity as a function of Mg<sup>2+</sup> rejection for three

commercial NF membranes tested in this study and membranes reported in the literature. The selectivity has a strong dependence on  $Mg^{2+}$  rejection, especially when  $Mg^{2+}$  rejection is high. d, Li $^+/Mg^{2+}$  selectivity as a function of MLR, with the permeate Li purity (defined by equation (2)) presented in dashed lines (varies from 10% to 99%). Data points on the same dash line have the same purity. For all panels, circles represent data from literature studies, including polyamide membranes (legend: PA (lit.)) and polyelectrolyte membranes fabricated by layer-by-layer deposition (legend: LbL (lit.)); diamonds represent data collected in this study.

Table 1 | Performance comparison of two scenarios with the same Li/Mg selectivity

		Scenario 1	Scenario 2
Li/Mg selectivity		ţ	50
Purity	MLR: 10		83.3%
	MLR: 50		50.0%
Li* rejection		-80%	95%
Mg <sup>2+</sup> rejection		96.4%	99.9%
LiRª	WR: 50%	90%	2.5%
	WR: 80%	144%	4.0%

 $<sup>^{</sup>a}$ The lithium recovery (LiR) calculated here is based on the to-be-disproved assumption of WR-independent Li $^{+}$  and Mg $^{2+}$  rejections.

partition and diffusion coefficients (Supplementary Text 1)<sup>29</sup>. The ion flux for species i,  $J_i$ , in the SDEM model is described using the modified Nernst–Planck equation:

$$J_i = -P_i \left( \frac{\mathrm{d}c_i}{\mathrm{d}x} + z_i c_i \frac{\mathrm{d}\varphi}{\mathrm{d}x} \right) \tag{5}$$

where  $P_i$  is the ion permeability,  $c_i$  is the ion concentration in the virtual solution, x is the transmembrane coordinate normalized by the membrane thickness,  $z_i$  is the valence of species i, and  $\varphi$  is the local electrical potential in the virtual solution. Solving equation (5) yields the transmembrane distributions of ion concentrations, electrical potential and electrical field (Fig. 3a as an illustration), which enables calculating rejections in a local differential element.

The SDEM model is semi-empirical because  $P_i$  is not constant but has a rather complex dependence on the feed composition. While more mechanistic models are capable of describing multi-component transport<sup>30,31</sup>, they usually contain questionable assumptions and many fitting parameters. For simplicity, we employ a linear correlation to relate  $P_i$  to feed composition:

$$P_i = \alpha_1 c'_{f,Li} + \alpha_2 c'_{f,Mg} + \alpha_3 \tag{6}$$

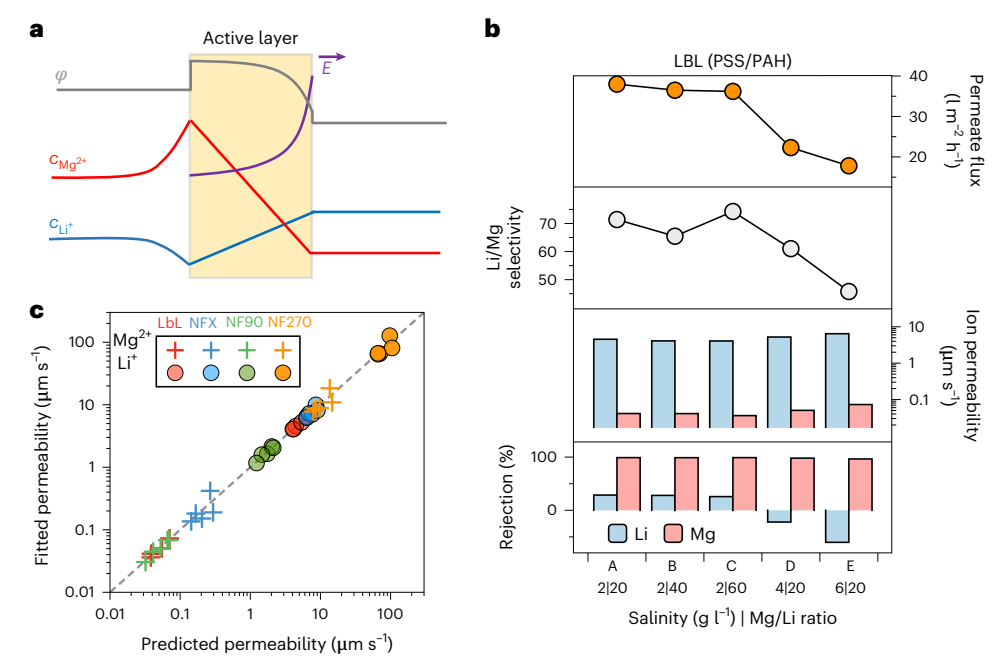


**Fig. 3** | **Application of the SDEM model to describe NF-based Li/Mg separation. a**, Representative distributions of electrical potential  $(\varphi)$ , electric field  $(\vec{E})$ , and concentrations of  $Mg^{2+}(C_{Mg}^2+)$  and  $Li^*(C_{Li^*})$  across the active layer of a positively charged NF membrane. **b**, From top to bottom: permeate water flux,  $Li^*/Mg^{2+}$  selectivity, fitted ion permeabilities and measured rejections as a function of feed composition. The composition comprises both total concentration (in grams per litre) and  $Mg^{2+}/Li^*(mass)$  ratio. Rejections and flux

data were reported in He et al.'s study<sup>24</sup>. Li\*/Mg<sup>2+</sup> selectivity was calculated with equation (1). Ion permeabilities were fitted with the SDEM model.  $\mathbf{c}$ , Fitted permeability extracted from the SDEM model using experimental data versus the predicted permeability obtained using the empirical correlation presented in equation (6) for three commercial NF membranes tested in this study and the LbL polyelectrolyte membrane in He et al.'s study<sup>24</sup>. CP was accounted for by an assumed mass transfer coefficient of  $100 \text{ I m}^{-2} \text{ h}^{-1}$  for both LiCl and MgCl<sub>2</sub>.

where  $c_{\rm f,Li}'$  and  $c_{\rm f,Mg}'$  are the local interfacial feed concentrations of Li<sup>+</sup> and Mg<sup>2+</sup>, and  $\alpha_{\rm j}$  are fitting coefficients. We note that the linear correlation works well in this analysis but requires further validation before applying to a more complex mixture feed solution. The local interfacial concentrations relate to the local bulk concentrations via concentration polarization (CP):

$$\frac{c'_{f,i} - c_{p,i}}{c_{f,i} - c_{p,i}} = \exp\left(\frac{J_w}{k_i}\right) \tag{7}$$

where  $J_w$  is local water flux and  $k_i$  is the mass transfer coefficient of species  $i.J_w$  can be estimated using

$$J_{\rm w} = P_{\rm w} \left( \Delta P - \Delta \pi_{\rm m} \right) \tag{8}$$

where  $P_{\rm w}$  is the water permeability, and  $\Delta P$  and  $\Delta \pi_{\rm m}$  are the transmembrane difference of hydrostatic pressure and osmotic pressure, respectively. For relatively dilute solutions, the van't Hoff equation can be applied to relate  $\Delta \pi_{\rm m}$  to transmembrane concentration differences (Methods). The local mass transfer can be determined by solving equations (5–8) simultaneously with charge neutrality and steady-state conditions.

We use the data of water flux and ion rejections of a polyelectrolyte membrane coupon measured with different feed compositions (Fig. 3b) as reported by He et al.  $^{24}$  to extract the permeability of Li $^{+}$  ( $P_{\rm Li}$ ) and Mg $^{2+}$  ( $P_{\rm Mg}$ ) and determine the correlation coefficients in equation (6). The polyelectrolyte membrane (named LbL in Fig. 3b,c) was fabricated using layer-by-layer (LbL) deposition of poly sodium (4-styrenesulfonate) and poly(allylamine) hydrochloride $^{24}$ . Additionally, we measured the performance of commercial NF membranes using the conditions (Methods and Supplementary Fig. 1). The correlations of ion permeability for these membranes are summarized in Supplementary Table 3. In general,  $P_{\rm Li}$  is one to two orders of magnitude higher than

 $P_{\rm Mg}$ , and the linear correlations can provide reasonable predictions of the permeabilities extracted from the SDEM model using experimental data (Fig. 3c).

With a model to evaluate the local mass transfer in a differential element, we can now extend the analysis to module scale by numerically integrating the governing differential equations for species conservation over a finite membrane area (Methods). Here we based our illustrative analysis on the polyelectrolyte membrane and generate representative results to describe the module-scale behaviours in NF-based Li/Mg separation. Intuitively, the module behaviour can be described as a spatial distribution of solution properties and separation performance along the direction of the feed flow. However, a more universal representation is to replace the position in the module with WR (up to that position) because WR increases as feed water flows past more membrane area.

As more water is recovered, the Mg<sup>2+</sup> concentration in the retentate (that is, the solution remaining in the feed channel after partial water recovery) increases dramatically, whereas the retentate Li<sup>+</sup> concentration first increases and then decreases but overall remains low (Fig. 4a). The permeate concentrations of Li<sup>+</sup> and Mg<sup>2+</sup> consistently increase with increasing WR (Fig. 4b). Here we distinguish between the local and cumulative permeate concentrations: the local concentrations are what could have been measured using a membrane coupon with the local feed composition, whereas the cumulative concentrations consider the cumulative ion and water permeation preceding the position corresponding to the current WR (that is,  $\int J_i dS / \int J_w dS$ , where dS is the differential membrane area). Correspondingly, the Li<sup>+</sup> and Mg<sup>2+</sup> rejections can also be defined locally and cumulatively (Fig. 4c). While the local Li<sup>+</sup> rejection can become strongly negative (as observed with some membrane coupons), the cumulative Li<sup>+</sup> rejection cannot, thereby preventing the erroneous inference of over 100% LiR presented in Table 1.

The non-monotonic dependence of retentate Li<sup>+</sup> concentration on WR (Fig. 4a inset) is a direct result of local Li<sup>+</sup> rejection transitioning

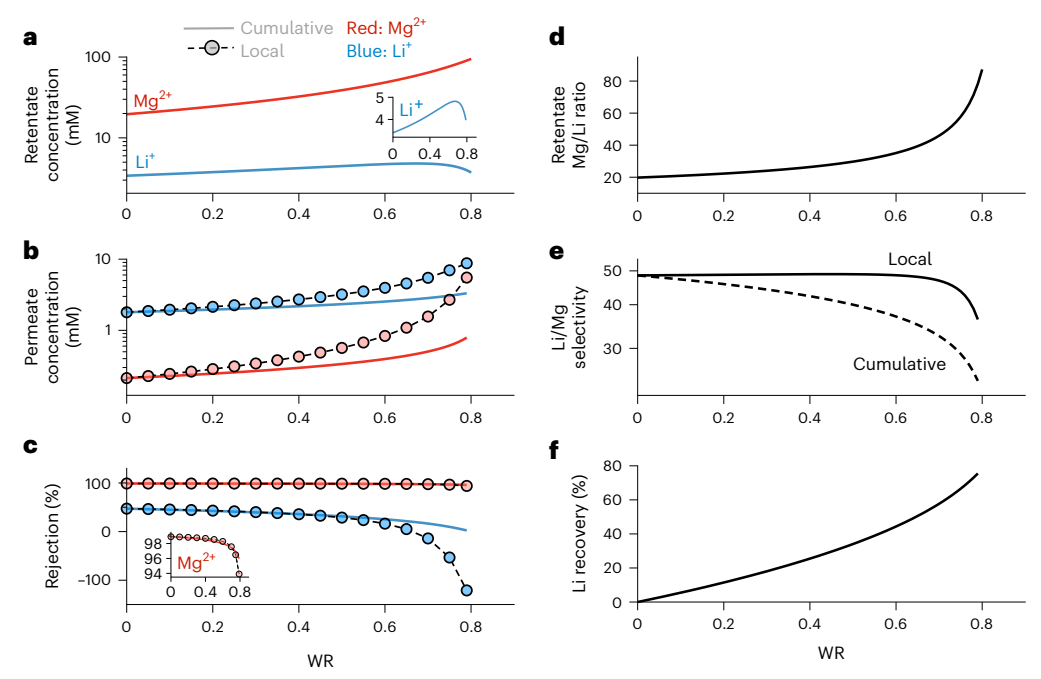


Fig. 4 | Representative results from module-scale modelling of NF-based Li/Mg separation. a-c, Retentate concentrations (inset is the magnified Li $^{\dagger}$  curve) (a), permeate concentrations (b) and rejections (inset is the magnified Mg $^{2+}$  curve) (c) as a function of water recovery (WR). The dashed curves with circles represent 'local values', whereas the solid curves present 'cumulative values'. In b, for example, the local concentration is obtained by applying the SDEM model to a differential module element using the retentate concentration at the same position (as in a), whereas the cumulative concentration is obtained

considering accumulation of ions from the permeate stream entering the differential module element. In  $\mathbf{c}$ , the local and cumulative rejections are calculated using the local and cumulative concentrations in  $\mathbf{b}$ , respectively.  $\mathbf{d}-\mathbf{f}$ , Retentate MLR ( $\mathbf{d}$ ), local and cumulative Li/Mg selectivity ( $\mathbf{e}$ ) and Li recovery ( $\mathbf{f}$ ) as a function of WR. Simulation used 6 bar and a feed solution of LiCl and MgCl<sub>2</sub> with 2 g l<sup>-1</sup> total concentration and MLR of 20. CP was accounted for by a mass transfer coefficient of 100 l m<sup>-2</sup> h<sup>-1</sup> for both LiCl and MgCl<sub>2</sub>.

from positive to negative as WR increases (Fig. 4c). Despite the low (but positive)  $R_{1i}$  at low WR, the Li<sup>+</sup> in the retentate is still concentrated with more water recovered, until  $R_{ij}$  becomes negative at high WR. The strongly negative rejection of Li<sup>+</sup> at high WR is a result of both high local MLR ratio (Fig. 4d) and low local water flux due to diminishing driving force with increasing retentate osmotic pressure (Supplementary Fig. 2). Notably, both the cumulative selectivity and local selectivity drop with increasing WR (Fig. 4e) despite the progressively more favourable Li<sup>+</sup> permeation at higher WR (Fig. 4c), which can be explained by the noticeable reduction of  $R_{Mg}$  with increasing WR (Fig. 4c inset) and the high sensitivity of  $S_{\text{Li/Mg}}$  to  $R_{\text{Mg}}$  (equation (1)). The drop in local Li/Mg selectivity is a result of both the varying retentate composition (Fig. 4a) and water flux, as selectivity could be substantially compromised when the water flux is too low (Supplementary Text 2 and Supplementary Fig. 3). Lastly, Li recovery, LiR, increases monotonically as more water is recovered (Fig. 4f).

#### Performance trade-off in NF operation

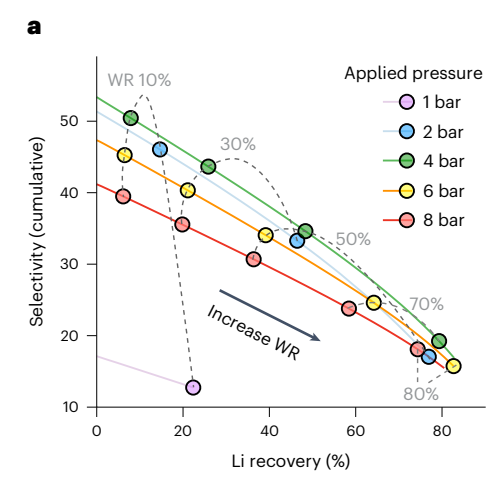
From an operational perspective, the module-scale analysis reveals an intrinsic trade-off between the (cumulative) selectivity,  $S_{\rm Li/Mg}$ , and Li recovery, LiR. For a single-stage NF process with a given applied pressure and influent feed flowrate, a higher WR can be achieved by providing more membrane area. Increasing WR increases LiR (Fig. 4f) but at the cost of reduced  $S_{\rm Li/Mg}$  (Fig. 4e), resulting in the trade-off between  $S_{\rm Li/Mg}$  and LiR (Fig. 5a).

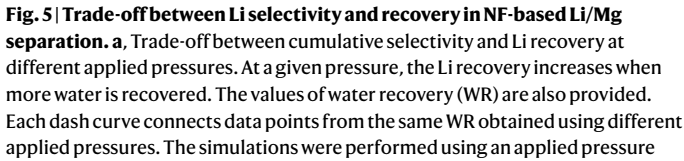
The characteristic curve quantifying the trade-off between  $S_{\text{Li/Mg}}$  and LiR, namely the operational trade-off curve, depends on the applied pressure,  $\Delta P$ , which affects the water flux. At a low  $\Delta P$ , water permeates through the membrane at a lower rate. However, the ion fluxes are not affected proportionally due to the negligible advective ion transport in NF. Therefore, operating NF at lower  $\Delta P$  enhances the

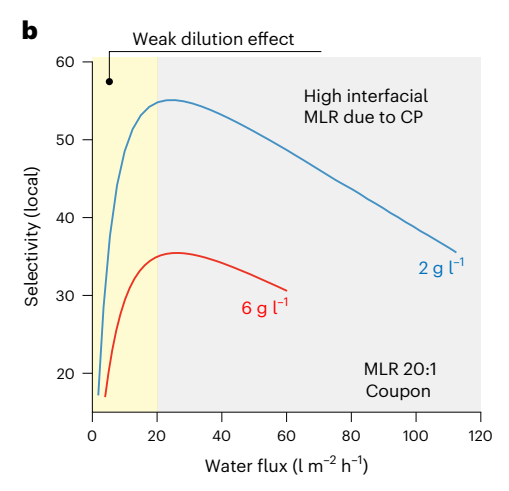
relative Li<sup>+</sup> permeation as compared with water permeation, which results in a higher LiR at the same WR and thereby shifts the trade-off curve towards the right (see dash curves in Fig. 5a). This effect of enhanced LiR at the same WR is more prominent at a higher WR. Notably, the maximum WR achievable with unlimited membrane area is also dependent on  $\Delta P$ , as water permeation stops when  $\Delta \pi_{\rm m}$  reaches  $\Delta P$ . In the extreme case of applying only 1 bar, the maximum attainable WR and LiR are -10% and -22%, respectively.

In the range of low WR,  $S_{\text{Li/Mg}}$  increases considerably as  $\Delta P$  decreases from 8 bar to 4 bar, that is, reducing  $\Delta P$  and water flux in this range also shifts the trade-off curves up (Fig. 5a). However, further reducing  $\Delta P$  below 4 bar compromises  $S_{\text{Li/Mg}}$  (see reflection of dash curves in Fig. 5a). With a  $\Delta P$  of 1 bar,  $S_{\text{Li/Mg}}$  becomes very low. While the cumulative selectivity,  $S_{\text{Li/Mg}}$ , has a complex dependence on multiple factors (for example, water flux and feed composition) that varies along the module, the non-monotonic dependence of  $S_{\text{Li/Mg}}$  can be explained by the flux dependence of local selectivity as shown in Fig. 5b.

In the water flux regime typical of NF (grey region in Fig. 5b), local Li/Mg selectivity decreases monotonically with increasing water flux due to CP. Specifically, because  $Mg^{2^+}$  ions are far better rejected than Li<sup>+</sup> ions, the accumulation of  $Mg^{2^+}$  near the membrane surface is more severe than Li<sup>+</sup>, which results in a higher interfacial MLR at a higher water flux (Supplementary Fig. 4). A higher interfacial MLR is detrimental to local Li/Mg selectivity, which is strongly sensitive to  $Mg^{2^+}$  rejection, because a heightened interfacial  $Mg^{2^+}$  concentration compromises  $Mg^{2^+}$  rejection (Supplementary Fig. 5). In the very low water flux regime (yellow region in Fig. 5b, untypical of NF), local Li/Mg selectivity drops dramatically with decreasing water flux due to the substantially reduced rejections of all ions because of the weakened 'dilution effect'. As  $S_{\text{Li/Mg}}$  is much more sensitive to  $Mg^{2^+}$  rejection than to Li<sup>+</sup> rejection, reducing the rejections of all ions leads to a dramatic drop in  $S_{\text{Li/Mg}}$ .







of 1, 2, 4, 6 and 8 bar and a feed solution of LiCl and MgCl $_2$  with 2 g l $^{-1}$  total concentration and an MLR of 20. **b**, Coupon-scale selectivity as a function of water flux with a feed MLR of 20 and a total concentration of 2 g l $^{-1}$  and 6 g l $^{-1}$ . The applied pressure varies up to 10 bar to vary the water flux. CP was accounted for by an assumed mass transfer coefficient of 100 l m $^{-2}$  h $^{-1}$  for both LiCl and MgCl $_2$ .

As selectivity is related to the permeate Li purity,  $\eta_{\text{Li}}$ , via equation (3), the trade-off between  $S_{\text{Li/Mg}}$  and LiR presented in Fig. 5a can be directly converted to a trade-off between  $\eta_{\text{Li}}$  and LiR for a given feed MLR (Supplementary Fig. 6). At a given applied pressure, the trade-off between the two important performance metrics in Li/Mg separation suggests that recovering more Li<sup>+</sup> by using a larger membrane area will inevitably yield a permeate stream with a lower  $\eta_{\text{Li}}$ . Within the typical range of NF flux,  $S_{\text{Li/Mg}}$  and LiR can be simultaneously improved by operating NF at a lower pressure to reduce water flux. Additionally, the trade-off curve can also be shifted towards a more favourable direction when a better membrane is used, with the definition of 'better' to be discussed below.

## Performance metrics of NF membrane for Li/Mg separation

What exactly is a 'better membrane' in the context of Li/Mg separation is an important question to the vibrant and growing community for developing high-performance NF membranes for Li/Mg separation. While many previous papers in this field compare membrane performance in a plot of Li/Mg selectivity versus water permeability ( $S_{\rm Li/Mg}$  versus  $P_{\rm w}$ ; Table 1), we have demonstrated why  $S_{\rm Li/Mg}$  is an insufficient metric. We have also shown that a high water flux is detrimental to both Li selectivity (or purity) and recovery (Fig. 5). Therefore, a high  $P_{\rm w}$  seems at odds with the success criteria for Li/Mg separation.

Selectivity is defined on the basis of rejections, which are less intrinsic than permeabilities, whereas membrane performance is more commonly quantified on the basis of permeabilities. Although one may rightfully argue that permeabilities are also not entirely intrinsic properties, they are more intrinsic than rejections and are adopted in the most widely used framework for evaluating membrane performance for water–solute separation. Selectivity in water–solute separation is defined on the basis of the ratio between water permeability  $(P_{\rm w})$  and solute permeability  $(P_{\rm s})$ . The water/solute selectivity  $(P_{\rm w}/P_{\rm s})$  is usually plotted against the water permeability  $(P_{\rm w})$  to illustrate the perm-selectivity of membranes<sup>7,32,33</sup>. However, such a performance evaluation framework based on  $P_{\rm w}/P_{\rm s}$  versus  $P_{\rm w}$  is clearly inappropriate for Li/Mg separation with very different success criteria compared with water–solute separation.

Not only should an ideal NF membrane for Li/Mg separation enable fast Li  $^{\dagger}$  transport and slow Mg  $^{2+}$  transport so that selective permeation

of Li<sup>+</sup> over Mg<sup>2+</sup> can be achieved to maximize Li purity, but it should also favour Li<sup>+</sup> permeation over water permeation to promote Li recovery. If water permeation is very fast yet Li<sup>+</sup> permeation is very slow, only a small fraction of Li<sup>+</sup> in the feed solution will end up in the permeate. Given these considerations, we propose that the performance of an NF membrane for Li/Mg separation should be evaluated on the basis of two permeability ratios,  $P_{\rm Li}/P_{\rm Mg}$  and  $P_{\rm Li}/P_{\rm W}$  (Fig. 6a). A high  $P_{\rm Li}/P_{\rm Mg}$  favours Li/Mg selectivity and Li purity, whereas a high  $P_{\rm Li}/P_{\rm w}$  favours Li recovery. These two permeability ratios directly correspond to the two success criteria in NF-based Li/Mg separation.

Like water–solute separation, a membrane with a higher  $P_{\rm w}$  can reduce the energy consumption and/or membrane area for a given feed flowrate, thereby reducing overall cost of the separation<sup>3,8</sup>. In Li/Mg separation, however, a higher  $P_{\rm w}$  is beneficial only if it does not compromise  $P_{\rm Li}/P_{\rm w}$ , because LiR is probably a more important performance metric than water flux or volume-specific energy consumption. In a bubble plot of  $P_{\rm Li}/P_{\rm Mg}$  versus  $P_{\rm Li}/P_{\rm w}$ , where  $P_{\rm w}$  may be quantified by the size of the 'bubbles' (Fig. 6a), an ideal membrane is a 'big bubble' on the upper right of the plot. The concept of a performance upper bound commonly employed for perm-selectivity in water–solute separation also applies here to describe the trade-off between Li purity and recovery. Future studies on developing high-performance NF membranes should aim to populate the bubble plot beyond the current upper bound.

The  $P_{\rm Li}/P_{\rm Mg}$  versus  $P_{\rm Li}/P_{\rm w}$  bubble plot should be used with caution when comparing membrane performance. Ideally, all data points in this plot should be obtained using the same feed composition and operating conditions, which is not necessarily the case across different studies. These testing conditions impact membrane performance, which is evident from the mild scattering of performance for a given membrane tested in different conditions (Fig. 6a and Supplementary Table 4). Future studies on membrane development should converge to a unified testing protocol for performance comparison on the  $P_{\rm Li}/P_{\rm Mg}$  versus  $P_{\rm Li}/P_{\rm w}$  bubble plot.

## Extending performance metrics of NF membrane for recovering ions in the brine

While the current analysis primarily focuses on Li extraction where the ions enriched in the permeate (that is, Li $^+$ ) are the product, the analysis framework can readily be extended to other selective solute separation where the ions retained in brine are the product (for example, rare

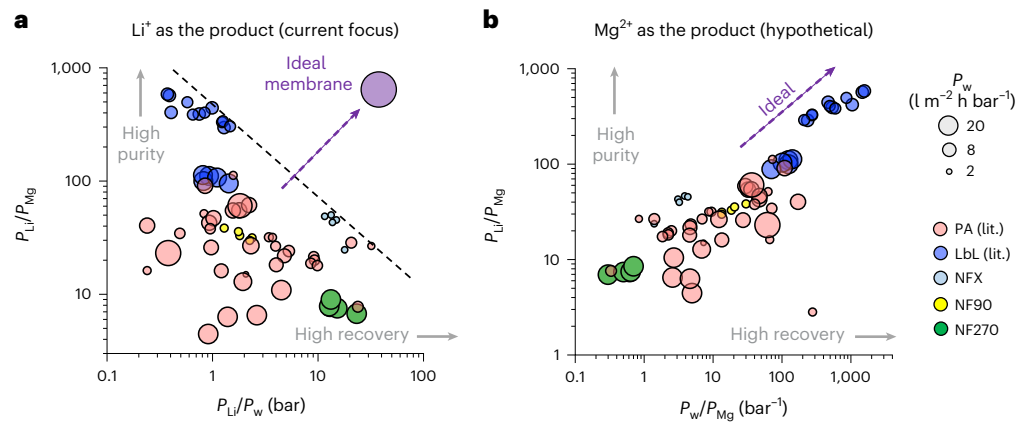


**Fig. 6** | **Performance metrics of NF membrane for Li/Mg separation (with either permeate or retentate as the product). a**, Ratio between Li permeability and Mg permeability ( $P_{\rm Li}/P_{\rm Mg}$ ) versus ratio between Li permeability and water permeability ( $P_{\rm Li}/P_{\rm w}$ ). This evaluation framework applies to extracting Li, or more generally, the ions enriched in the permeate. Increasing  $P_{\rm Li}/P_{\rm w}$  improves Li recovery, whereas increasing  $P_{\rm Li}/P_{\rm Mg}$  enhances permeate Li purity. **b**, Ratio between Li permeability and Mg permeability ( $P_{\rm Li}/P_{\rm Mg}$ ) versus ratio between water

permeability and Mg permeability ( $P_{\rm w}/P_{\rm Mg}$ ). This evaluation framework applies to extracting Mg, or more generally, the ions enriched in the brine. The size of the data points quantifies the water permeability,  $P_{\rm w}$  (see legend). The permeabilities are extracted using the SDEM model with an assumed mass transfer coefficient of  $100\,\rm l\,m^{-2}\,h^{-1}$  for both LiCl and MgCl<sub>2</sub>. Legends 'PA (lit.)' and 'LbL (lit.)' refer to literature data obtained using polyamide membranes and polyelectrolyte membranes fabricated by layer-by-layer deposition.

earth metal recovery)34. Without collecting new sets of data for such applications, here we analyse the same dataset for Li/Mg separation but for a hypothetical scenario where Mg<sup>2+</sup> ions are the product (Fig. 6b). The success criteria for such an application are clearly Mg purity and recovery. Analogous to how we evaluate membrane performance for Li extraction, here the  $P_{Li}/P_{Mg}$  ratio remains important as it determines the Mg purity in the brine stream. Unlike Li extraction, however, the relevant membrane property to Mg recovery is  $P_{\rm w}/P_{\rm Mg}$ . A high water permeability,  $P_{w}$ , not only improves performance from an energy or kinetic perspective as in conventional water-solute separation, but also benefits Mg recovery by ensuring that only a small fraction of Mg<sup>2+</sup> ions in the feed stream will end up in the permeate stream when most water permeates through the membrane. These two membrane performance metrics for Mg recovery using NF-based Li/Mg separation,  $P_{Li}/P_{Mg}$  and  $P_{w}/P_{Mg}$ , positively correlate with each other on the basis of data evaluated from literature using the SDEM model (Fig. 6b). In other words, there is no trade-off at the membrane level when NF-based Li/Mg separation is used towards Mg recovery.

#### Perspectives and outlook

Our analysis demonstrates that the existing framework for evaluating NF performance in water treatment is inadequate for quantifying NF performance for selective solute–solute separation. The performance metrics in the existing framework mismatch the success criteria for selective solute–solute separation when the goal is to extract a target solute as the desired product. Li/Mg separation is chosen as an example for illustrating such a mismatch and for developing a suitable framework for evaluating process and membrane performance. In NF-based Li/Mg separation, the key performance metrics at the process level should be Li/Mg selectivity (or Li purity) and Li recovery, not water permeability as currently used. The consideration of these two metrics results in important trade-off relations for operation optimization and membrane development.

From an operation perspective, process optimization of NF for Li/Mg separation should focus on Li purity and recovery, which are constrained by a trade-off relation (Fig. 5). Factors that are critical in water treatment, such as energy consumption and membrane cost, are probably less important in Li/Mg separation due to Li being a commodity with a much higher economic value than water. From membrane development perspective, NF membranes for Li/Mg separation should

be evaluated using the  $P_{\rm Li}/P_{\rm Mg}$  versus  $P_{\rm Li}/P_{\rm w}$  bubble plot (Fig. 6), which captures membrane properties most relevant to the success criteria of Li/Mg separation.

We also demonstrate how this analysis framework can readily extend to another general category of selective solute separation where ions in the brine are the target ions of extraction. We believe this general analysis framework featuring target ion purity and recovery will guide future endeavours in process innovation and optimization and the development of high-performance NF membranes for selective solute-solute separation.

#### Methods

#### Modelling module-scale performance with the SDEM model

The SDEM model describes local ion transport across the membrane with the modified Nernst–Planck equation (equation (5) in the main text). With a given feed solution composition and a set of ion permeabilities, permeate composition can be solved as a function of permeate flux with the charge neutrality (equation (9)) and steady-state (equation (10)) conditions:

$$\sum_{i} z_i c_i = 0 \tag{9}$$

$$J_i = J_{\mathbf{w}} c_{\mathbf{n},i} \tag{10}$$

where  $c_i$  is the concentration of ion i in the virtual solution or the external feed and permeate, and  $c_{p,i}$  is permeate concentration of ion i. Yaroshchuk and Bruening provided an analytical solution of the SDEM model for a ternary electrolyte system<sup>29</sup>. Thus, a pair of ion permeabilities can be fitted to describe the coupon-scale ion transport behaviour after accounting for CP (equation (7) in the main text), given experimental results of Li<sup>+</sup> and Mg<sup>2+</sup> rejections at a certain permeate flux. A MATLAB application is provided as Supplementary Code for fitting ion permeabilities.

The module behaviour was then modelled via a finite difference method to relate mass transfer in differential elements. Each differential element has either the same membrane area or the same increment of water recovery (WR). Since WR increases as feed water flows past more membrane area, the module-scale behaviours can be equivalently modelled as a function of WR instead of a function of

position along the module. The inputs were the applied pressure and the initial feed solution composition.

The modified Nernst–Planck equation (equation (5) in the main text) and the local permeate flux (equation (8) in the main text) were solved iteratively with ion permeabilities as a function of interfacial feed solution composition (equation (6) in the main text) to determine the local permeate composition and thus local ion rejections. Species conservation was maintained in the retentate and permeate when coupling the adjacent differential elements:

$$c_{p,i}^{loc}(WR) = \frac{d\left((1 - WR) c_{b,i}(WR)\right)}{dWR}$$
(11)

where  $c_{p,i}^{\rm loc}(WR)$  and  $c_{b,i}(WR)$  are local permeate concentration and bulk retentate (or brine, subscript 'b' for brine) concentration of ion i at water recovery WR, respectively. Cumulative permeate concentration,  $c_{p,i}^{\rm cum}(WR)$ , can be calculated as:

$$c_{p,i}^{\text{cum}}(WR) = \frac{\int c_{p,i}^{\text{loc}}(WR)dWR}{WR}$$
(12)

Local and cumulative rejections were then calculated by:

$$R_i^{\text{loc}}(WR) = 1 - \frac{c_{p,i}^{\text{loc}}(WR)}{c_{b,i}(WR)}$$
 (13a)

$$R_i^{\text{cum}}(WR) = 1 - \frac{c_{p,i}^{\text{cum}}(WR)}{c_{f,i}}$$
 (13b)

where  $c_{f,i}$  is the initial (or influent) feed concentration of ion *i*. Local and cumulative selectivity can also be determined according to equation (1) in the main text.

## Estimation of osmotic pressure of the LiCl-MgCl $_2$ mixed electrolyte solution

For relatively dilute solutions, the van't Hoff equation is usually applied to estimate the solution osmotic pressure:

$$\pi = RT \sum_{i} \frac{c_i}{MW_i} \tag{14}$$

where  $c_i$  is ion mass concentration of ion i,  $MW_i$  is the molecular weight of ion i, R is ideal gas constant and T is solution temperature. Transmembrane osmotic pressure,  $\Delta \pi_{\rm m}$ , can be then estimated with feed side interfacial concentrations and permeate concentrations:

$$\Delta \pi_{\rm m} = RT \sum_{i} \frac{(c_{\rm fm,i} - c_{\rm p,i})}{MW_{i}}$$
 (15)

We note that, if solution non-ideality is accounted for, ion permeance should be estimated in terms of ion activity gradient rather than concentration gradient. Ion activity coefficient and solution osmotic pressure can be estimated by the Pitzer model  $^{35}$ .

## Li/Mg NF separation experiments using commercial membranes

Li/Mg NF separation experiments were carried out in a lab-customized crossflow filtration system with stainless-steel membrane coupons. Effective membrane area of each coupon is 7.1 cm². The crossflow rate is 2.7 l min⁻¹. Three commercial thin-film composite polyamide NF membranes, NFX (Synder) and NF90 and NF270 (Filmtec, Dow), were tested. Pure water permeability was first measured at 6 bar after pre-compaction of the membrane samples. Li/Mg separation was then conducted at 6 bar with both retentate and permeate streams

circulating back to the feed tank. The feed solutions were prepared with LiCl and  $\mathrm{MgCl}_2$  (Sigma-Aldrich) to achieve a total concentration of 2, 4 and 6 g l<sup>-1</sup>, and an MLR of 20, 40 and 60. After filtration reaches steady state, permeate flux was measured and permeate samples were collected for ion concentration measurements. Li<sup>+</sup> and  $\mathrm{Mg}^{2+}$  concentrations were measured by inductively coupled plasma optical emission spectroscopy. The permeate flux,  $J_{w}$ , of the NF experiments was determined using the following equation:

$$J_{\rm W} = \frac{\Delta V}{A_{\rm F} \Delta t} \tag{16}$$

where  $\Delta V$  is the permeate volume produced in the period of  $\Delta t$  and  $A_{\rm F}$  is the effective filtration area of the membrane coupon. The observed ion rejection,  $R_{ij}$  was calculated as

$$R_i = 1 - \frac{c_{p,i}}{c_{f,i}} \tag{17}$$

where  $c_{\rm p,i}$  and  $c_{\rm f,i}$  are concentrations of the target ion in the permeate and feed solution, respectively.

#### **Reporting summary**

Further information on research design is available in the Nature Portfolio Reporting Summary linked to this article.

#### **Data availability**

Source data are provided with the paper. Source data for figures are in Excel format (.xlsx) and also available publicly via https://doi.org/10.6084/m9.figshare.21944408.

#### **Code availability**

The code for generating Fig. 4 in the manuscript is available publicly via the following link: https://github.com/ruoyuwang16/NATWATER-22-0394-Data-and-Codes.

#### References

- Zhao, Y. et al. Differentiating solutes with precise nanofiltration for next generation environmental separations: a review. *Environ. Sci. Technol.* 55, 1359–1376 (2021).
- Epsztein, R., DuChanois, R. M., Ritt, C. L., Noy, A. & Elimelech, M. Towards single-species selectivity of membranes with subnanometre pores. *Nat. Nanotechnol.* 15, 426–436 (2020).
- 3. Werber, J. R., Deshmukh, A. & Elimelech, M. The critical need for increased selectivity, not increased water permeability, for desalination membranes. *Environ. Sci. Technol. Lett.* **3**, 112–120 (2016).
- Elimelech, M. & Phillip, W. A. The future of seawater desalination: energy, technology, and the environment. Science 333, 712–717 (2011).
- Park, H. B., Kamcev, J., Robeson, L. M., Elimelech, M. & Freeman,
   B. D. Maximizing the right stuff: the trade-off between membrane permeability and selectivity. Science 356, 1138–1148 (2017).
- Werber, J. R., Porter, C. J. & Elimelech, M. A path to ultraselectivity: support layer properties to maximize performance of biomimetic desalination membranes. *Environ. Sci. Technol.* 52, 10737–10747 (2018).
- Yang, Z., Guo, H. & Tang, C. Y. The upper bound of thin-film composite (TFC) polyamide membranes for desalination. J. Memb. Sci. 590, 117297 (2019).
- 8. Yang, Z., Long, L., Wu, C. & Tang, C. Y. High permeance or high selectivity? Optimization of system-scale nanofiltration performance constrained by the upper bound. ACS ES&T Eng. 2, 377–390 (2022).

- Fang, W., Shi, L. & Wang, R. Interfacially polymerized composite nanofiltration hollow fiber membranes for low-pressure water softening. J. Memb. Sci. 430, 129–139 (2013).
- Labban, O., Liu, C., Chong, T. H., Lienhard, V. & John, H. Fundamentals of low-pressure nanofiltration: membrane characterization, modeling, and understanding the multi-ionic interactions in water softening. J. Memb. Sci. 521, 18–32 (2017).
- Wang, T., Han, H., Wu, Z., Dai, R. & Wang, Z. Humic acid modified selective nanofiltration membrane for efficient separation of PFASs and mineral salts. ACS ES&T Water 2, 1152–1160 (2022).
- Zhao, Y., Tong, X. & Chen, Y. Fit-for-purpose design of nanofiltration membranes for simultaneous nutrient recovery and micropollutant removal. *Environ. Sci. Technol.* 55, 3352–3361 (2021).
- Lin, J. et al. Toward resource recovery from textile wastewater: dye extraction, water and base/acid regeneration using a hybrid NF-BMED process. ACS Sustain. Chem. Eng. 3, 1993–2001 (2015).
- Li, X. et al. Membrane-based technologies for lithium recovery from water lithium resources: a review. J. Membr. Sci. 591, 117317 (2019).
- 15. Woong, J. et al. Hydrometallurgy recovery of lithium from Uyuni salar brine. *Hydrometallurgy* **117–118**, 64–70 (2012).
- Swain, B. Recovery and recycling of lithium: a review. Sep. Purif. Technol. 172, 388–403 (2017).
- Xu, S. et al. Extraction of lithium from Chinese salt-lake brines by membranes: design and practice. J. Membr. Sci. 635, 119441 (2021).
- 18. Xu, P., Hong, J., Xu, Z., Xia, H. & Ni, Q. Novel aminated graphene quantum dots (GQDs-NH<sub>2</sub>)-engineered nanofiltration membrane with high Mg<sup>2+</sup>/Li<sup>+</sup> separation efficiency. Sep. Purif. Technol. **258**, 118042 (2021).
- Yang, Z., Fang, W., Wang, Z., Zhang, R. & Zhu, Y. Dual-skin layer nanofiltration membranes for highly selective Li<sup>+</sup>/Mg<sup>2+</sup> separation. J. Membr. Sci. 620, 118973 (2021).
- Bi, Q., Zhang, C., Liu, J., Liu, X. & Xu, S. Positively charged zwitterion-carbon nitride functionalized nanofiltration membranes with excellent separation performance of Mg<sup>2+</sup>/Li<sup>+</sup> and good antifouling properties. Sep. Purif. Technol. 257, 117959 (2021).
- Xu, P. et al. 'Bridge' graphene oxide modified positive charged nanofiltration thin membrane with high efficiency for Mg<sup>2+</sup>/Li<sup>+</sup> separation. Desalination 488, 114522 (2020).
- Shen, Q., Xu, S., Xu, Z.-L., Zhang, H.-Z. & Dong, Z.-Q. Novel thin-film nanocomposite membrane with water-soluble polyhydroxylated fullerene for the separation of Mg<sup>2+</sup>/Li<sup>+</sup> aqueous solution. *J. Appl. Polym. Sci.* 136, 48029 (2019).
- 23. Guo, C. et al. Amino-rich carbon quantum dots ultrathin nanofiltration membranes by double 'one-step' methods: breaking through trade-off among separation, permeation and stability. *Chem. Eng. J.* **404**, 127144 (2021).
- 24. He, R. et al. Unprecedented Mg<sup>2+</sup>/Li<sup>+</sup> separation using layer-by-layer based nanofiltration hollow fiber membranes. *Desalination* **525**, 115492 (2022).
- Wang, R., Zhang, J., Tang, C. Y. & Lin, S. Understanding selectivity in solute-solute separation: definitions, measurements, and comparability. *Environ. Sci. Technol.* 56, 2605–2616 (2022).
- 26. Yaroshchuk, A. E. Negative rejection of ions in pressure-driven membrane processes. *Adv. Colloid Interface Sci.* **139**, 150-173 (2008).
- Yaroshchuk, A., Bruening, M. L. & Zholkovskiy, E. Modelling nanofiltration of electrolyte solutions. *Adv. Colloid Interface Sci.* 268, 39–63 (2019).
- Yaroshchuk, A., Bruening, M. L., Eduardo, E. & Bernal, L. Solution-diffusion-electro-migration model and its uses for analysis of nanofiltration, pressure-retarded osmosis and forward osmosis in multi-ionic solutions. *J. Membr. Sci.* 447, 463–476 (2013).

- 29. Yaroshchuk, A. & Bruening, M. L. An analytical solution of the solution-diffusion-electromigration equations reproduces trends in ion rejections during nanofiltration of mixed electrolytes. *J. Membr. Sci.* **523**, 361–372 (2017).
- Osorio, S. C., Biesheuvel, P. M., Dykstra, J. E. & Virga, E. Nanofiltration of complex mixtures: the effect of the adsorption of divalent ions on membrane retention layer. *Desalination* 527, 115552 (2022).
- Wang, R. & Lin, S. Pore model for nanofiltration: history, theoretical framework, key predictions, limitations, and prospects. J. Membr. Sci. 620, 118809 (2021).
- Geise, G. M., Park, H. B., Sagle, A. C., Freeman, B. D. & McGrath, J. E. Water permeability and water/salt selectivity tradeoff in polymers for desalination. J. Membr. Sci. 369, 130–138 (2011).
- Ritt, C. L. et al. The open membrane database: synthesisstructure-performance relationships of reverse osmosis membranes. J. Membr. Sci. 641, 119927 (2022).
- 34. Zhao, Z. et al. Exploring ions selectivity of nanofiltration membranes for rare earth wastewater treatment. *Sep. Purif. Technol.* **289**, 120748 (2022).
- Pitzer, K. S. & Kim, J. J. Thermodynamics of electrolytes. IV. Activity and osmotic coefficients for mixed electrolytes. J. Am. Chem. Soc. 96, 5701–5707 (1974).

#### Acknowledgements

The authors acknowledge the support from the US National Science Foundation (#2017998), Water Research Foundation (Paul L. Busch Award to S.L.), US-Israel Binational Agricultural Research and Development Fund (BARD IS-5209-19) and the National Natural Science Foundation of China (#U20A20139).

#### **Author contributions**

R.W. and S.L. conceived the idea and designed the research. R.W. conducted the quantitative analysis. All authors participated in the discussion and writing of the paper.

#### **Competing interests**

The authors declare no competing interests.

#### **Additional information**

**Supplementary information** The online version contains supplementary material available at https://doi.org/10.1038/s44221-023-00037-0.

**Correspondence and requests for materials** should be addressed to Shihong Lin.

**Peer review information** *Nature Water* thanks Akshay Deshmukh, Jiangnan Shen and Jian Jin for their contribution to the peer review of this work.

**Reprints and permissions information** is available at www.nature.com/reprints.

**Publisher's note** Springer Nature remains neutral with regard to jurisdictional claims in published maps and institutional affiliations.

Springer Nature or its licensor (e.g. a society or other partner) holds exclusive rights to this article under a publishing agreement with the author(s) or other rightsholder(s); author self-archiving of the accepted manuscript version of this article is solely governed by the terms of such publishing agreement and applicable law.

© The Author(s), under exclusive licence to Springer Nature Limited 2023

# nature portfolio

Corresponding author(s):	Shihong Lin
Last updated by author(s):	Jan 19, 2023

## **Reporting Summary**

Nature Portfolio wishes to improve the reproducibility of the work that we publish. This form provides structure for consistency and transparency in reporting. For further information on Nature Portfolio policies, see our <u>Editorial Policies</u> and the <u>Editorial Policy Checklist</u>.

		1.5		
•	$r \sim$	TI	ST.	-
_ ``	ıa		<b>``</b>	

For a	ll statistical an	alyses, confirm that the following items are present in the figure legend, table legend, main text, or Methods section.			
n/a	Confirmed				
	The exact	sample size $(n)$ for each experimental group/condition, given as a discrete number and unit of measurement			
	A stateme	nt on whether measurements were taken from distinct samples or whether the same sample was measured repeatedly			
	The statistical test(s) used AND whether they are one- or two-sided  Only common tests should be described solely by name; describe more complex techniques in the Methods section.				
	A descript	ion of all covariates tested			
$\boxtimes$	A description of any assumptions or corrections, such as tests of normality and adjustment for multiple comparisons				
	A full description of the statistical parameters including central tendency (e.g. means) or other basic estimates (e.g. regression coefficient) AND variation (e.g. standard deviation) or associated estimates of uncertainty (e.g. confidence intervals)				
	For null hypothesis testing, the test statistic (e.g. <i>F</i> , <i>t</i> , <i>r</i> ) with confidence intervals, effect sizes, degrees of freedom and <i>P</i> value noted Give <i>P</i> values as exact values whenever suitable.				
	For Bayesi	an analysis, information on the choice of priors and Markov chain Monte Carlo settings			
	For hierar	chical and complex designs, identification of the appropriate level for tests and full reporting of outcomes			
	Estimates of effect sizes (e.g. Cohen's $d$ , Pearson's $r$ ), indicating how they were calculated				
Our web collection on <u>statistics for biologists</u> contains articles on many of the points above.					
Software and code					
Policy information about <u>availability of computer code</u>					
Dat	ta collection	MATLAB Online has been used to solve the mass transport model in the manuscript with customized codes.			
Data analysis MATLAB Online has been used to solve the mass transport model in the manuscrip		MATLAB Online has been used to solve the mass transport model in the manuscript with customized codes.			
For manuscripts utilizing custom algorithms or software that are central to the research but not yet described in published literature, software must be made available to editors and reviewers. We strongly encourage code deposition in a community repository (e.g. GitHub). See the Nature Portfolio guidelines for submitting code & software for further information.					

## Data

Policy information about availability of data

All manuscripts must include a data availability statement. This statement should provide the following information, where applicable:

- Accession codes, unique identifiers, or web links for publicly available datasets
- A description of any restrictions on data availability
- For clinical datasets or third party data, please ensure that the statement adheres to our policy

Provide your data availability statement here.

Human research part	icipants		
Policy information about studies	involving human research participants and Sex and Gender in Research.		
Reporting on sex and gender	The study doesn't involve human research participants.		
Population characteristics	opulation characteristics The study doesn't involve human research participants.		
Recruitment	The study doesn't involve human research participants.		
Ethics oversight	The study doesn't involve human research participants.		
Note that full information on the app	roval of the study protocol must also be provided in the manuscript.		
Field-specific reporting			
Please select the one below that is the best fit for your research. If you are not sure, read the appropriate sections before making your selection.			
Life sciences Behavioural & social sciences Ecological, evolutionary & environmental sciences			
For a reference copy of the document with all sections, see <a href="mailto:nature.com/documents/nr-reporting-summary-flat.pdf">nature.com/documents/nr-reporting-summary-flat.pdf</a>			
Ecological, evolutionary & environmental sciences study design			
All studies must disclose on these points even when the disclosure is negative.			

Study description

Briefly describe the study. For quantitative data include treatment factors and interactions, design structure (e.g., factorial, nested. hierarchical), nature and number of experimental units and replicates.

Research sample

Describe the research sample (e.g., a group of tagged Passer domesticus, all Stenocereus thurberi within Organ Pipe Cactus National Monument), and provide a rationale for the sample choice. When relevant, describe the organism taxa, source, sex, age range and any manipulations. State what population the sample is meant to represent when applicable. For studies involving existing datasets, describe the data and its source.

Sampling strategy

Note the sampling procedure. Describe the statistical methods that were used to predetermine sample size OR if no sample-size calculation was performed, describe how sample sizes were chosen and provide a rationale for why these sample sizes are sufficient.

Data collection

Describe the data collection procedure, including who recorded the data and how.

Timing and spatial scale

Indicate the start and stop dates of data collection, noting the frequency and periodicity of sampling and providing a rationale for these choices. If there is a gap between collection periods, state the dates for each sample cohort. Specify the spatial scale from which the data are taken

Data exclusions

If no data were excluded from the analyses, state so OR if data were excluded, describe the exclusions and the rationale behind them, indicating whether exclusion criteria were pre-established.

Reproducibility

Describe the measures taken to verify the reproducibility of experimental findings. For each experiment, note whether any attempts to repeat the experiment failed OR state that all attempts to repeat the experiment were successful.

Randomization

Describe how samples/organisms/participants were allocated into groups. If allocation was not random, describe how covariates were controlled. If this is not relevant to your study, explain why.

Blinding

Describe the extent of blinding used during data acquisition and analysis. If blinding was not possible, describe why OR explain why blinding was not relevant to your study.

Did the study involve field work?

Yes	
-----	--

No.

## Reporting for specific materials, systems and methods

We require information from authors about some types of materials, experimental systems and methods used in many studies. Here, indicate whether each material, system or method listed is relevant to your study. If you are not sure if a list item applies to your research, read the appropriate section before selecting a response.

ā
=
Ċ
CL
_
$\mathcal{Z}$
$\sim$
_
⊆
$\subseteq$
$\sim$
_
_
CL
7
−≽
-C

C	)
Е	
$\sim$	)
ш	
a	`
•	2
C	
$\subset$	)
	5
$\subseteq$	T.
7	ί.
٠	4
U	
ċ	
=	₹
=	5
Е	ξ.
Ξ	5
$\overline{\circ}$	
=	Ŕ
<	1

	2
١	$\stackrel{\sim}{\sim}$
Κ	_
Ľ	٥

Materials & experimental systems		Methods		
n/a	Involved in the study	n/a	Involved in the study	
$\boxtimes$	Antibodies	$\boxtimes$	ChIP-seq	
$\boxtimes$	Eukaryotic cell lines	$\boxtimes$	Flow cytometry	
$\boxtimes$	Palaeontology and archaeology	$\boxtimes$	MRI-based neuroimaging	
$\boxtimes$	Animals and other organisms			
$\boxtimes$	Clinical data			
$\boxtimes$	Dual use research of concern			